Reducible-Shell-Derived Pure-Copper-Nanowire Network and Its Application to Transparent Conducting Electrodes

*Hyewon Hwang, Areum Kim, Zhaoyang Zhong, Hyeok-Chan Kwon, Sunho Jeong, and Jooho Moon**

The concept of using core Cu nanowires (CuNWs) that are conformally encapsulated by a reducible fugitive material for transparent conducting electrodes (TCEs) with high oxidation stability is presented. By the chemical reaction of an acid with surface oxide and hydroxide, a uniform surface shell layer is readily obtained on each CuNW upon adding lactic acid to the CuNW dispersion. The Cu lactate shell prevents the core CuNW from oxidizing during storage and film formation, enabling the core Cu nanowires to maintain their characteristic optoelectronic properties. Through simple thermal annealing under a nitrogen atmosphere, the Cu lactate shell is easily decomposed to expose the underlying pure Cu, providing an effective way to produce a pure-CuNW-network TCE with a sheet resistance of 19.8 Ω sq^{-1} and an optical transmittance of 85.5% at 550 nm. The application of the CuNW-based TCE to the transparent top electrode in organometallic halide perovskite solar cells is further demonstrated for the first time, yielding a power-conversion efficiency 9.88% as compared to that of 13.39% for conventional perovskite solar cells with an indium–tin-oxide electrode. This study proposes the high feasibility of these CuNWs as a vacuum-free and noble-metal-free transparent-window electrode in perovskite solar cells.

1. Introduction

In recent years, copper nanowires (CuNWs) have attracted significant attention of researchers in both academia and industry, owing to their high electrical and thermal conductivity and unique anisotropic physicochemical properties. In contrast to silver, a highly expensive noble metal, copper is earth abundant and extremely inexpensive; thus, copper does not pose a cost burden in the mass production of large-scale devices that employ copper, such as transparent conducting electrodes (TCEs),[1–4] microheaters,[5] gas sensors, lithium-ion batteries,[6–8] solar cells,[9,10] and water-splitting catalysts.[11] In particular, as an alternative to conventional vacuum-deposited indium–tin oxide (ITO) and silver nanowires, CuNWs are a promising constituent material in TCEs based on random conductive networks. However, copper is easily oxidized even under ambient conditions, resulting in the formation of an insulating surface oxide layer and subsequent significant loss in electrical conductivity. From the viewpoint of practical applications, the chemical or physical reduction of copper oxides into a pure copper phase is a critical issue in the fabrication of highly conductive, copper-nanowire-based transparent electrodes.

To date, various reduction methods have been explored for the preparation of pure-CuNW-network films. The most commonly used method is heat treatment under a reductive atmosphere (e.g., a pure or diluted hydrogen gas, nitrogen gas bubbled through a formic acid), by which the surface oxide layer is easily reduced to the pure copper phase, with the formation of electrical junctions between neighboring nanowires. However, in practical applications with stacked device architectures, the incorporation of a chemically reductive atmosphere poses a significant hurdle to some extent, as it corrodes or erodes the underlying or encapsulating layers through unpredictable reactions such as impurity doping and contamination; therefore, safety is an important issue.

Wet acid treatments have been employed to chemically etch the surface oxide and hydroxide and to remove the remaining organic moieties. Stewart et al.[12] reported that by repeatedly dipping a CuNW film in an acetic acid bath, the acetic acid can eliminate the surface oxide layer and organic residues; but immersing a CuNW-network film in a rinsing solution likely decays the functional properties of other stacked layers and add to the process complexity in some cases. Won et al.[10] proposed that adding lactic acid to a CuNW suspension leads to dissolution of the surface oxide and hydroxide, transforming them into soluble species. However, the wet etching process should be kinetically controlled owing to a possible chemical reaction between the acid and central Cu phases, which can result in the morphological disconnection of nanowires. In addition, the bare surface is exposed to the ambient upon initiation of a wet chemical etching process, so subsequent procedures for TCE fabrication should be carried out immediately to prevent reoxidation along the nanowire surface at junction points. As an

H. Hwang, Dr. A. Kim, Z. Zhong, H.-C. Kwon, Prof. J. Moon
Department of Materials Science and Engineering
Yonsei University
50 Yonsei-ro, Seodaemun-gu
Seoul 120-749, Republic of Korea
E-mail: jmoon@yonsei.ac.kr
Dr. S. Jeong
Advanced Materials Division
Korea Research Institute of Chemical Technology
19 Sinseongno, Yuseong-gu
Daejeon 305-600, Republic of Korea

DOI: 10.1002/adfm.201602094

alternative, laser sintering and intense pulsed-light irradiation have been suggested to instantly reduce the surface layer via a photochemical reduction,[13–16] while the oxidation behavior is suppressed during the process and the CuNW film is heated instantaneously within nano- to microseconds, with the formation of electrical junctions between nanowires. However, these optothermal heating techniques require complex, expensive instruments for generating the highly energetic photons.

Here, we introduce reducible fugitive Cu-lactate shells that conformally encapsulate individual CuNWs; the Cu carboxylate layer is formed by a chemical reaction that consumes the surface oxide and hydroxide. The synthesis of such a Cu–Cu-lactate core–shell NW involves a very simple, cost-effective, high-throughput one-pot-solution procedure. The Cu carboxylate shell around a CuNW is easily decomposed to pure Cu by simple thermal annealing under an inert atmosphere, without leaving behind insulating by-products and organic residues. These noble Cu–Cu-lactate core–shell nanowires provide long-term oxidation stability even under a humid ambient atmosphere at an elevated temperature, and when dispersed in carrier solvents. We demonstrated that CuNWs with reducible fugitive shells provide an effective way to fabricate pure-CuNW-network TCEs with a sheet resistance of 19.8 Ω sq^{-1} and an optical transmittance of 85.5% at a wavelength of 550 nm.

In order to verify the applicability of our core–shell CuNWs in practical devices, we further demonstrated, for the first time, the possibility of using CuNWs as a top electrode in organometallic halide perovskite solar cells. Organometallic trihalide perovskites, especially methylammonium lead halides ($CH_3NH_3PbX_3$, X = Cl, I, Br), have attracted much attention as promising light-absorbing materials owing to their low cost, easy processability, and high photovoltaic performance (reaching 22.1% in power-conversion efficiency (PCE), certified by the National Renewable Energy Laboratory).[17] However, both the $CH_3NH_3PbX_3$ absorber layer and spiro-OMeTAD, which is widely used as a hole-transporting material (HTM), suffer from chemical dissolution when they are in contact with various solvents and are vulnerable to thermal damage. Such thermal- and chemical-sensitive natures of constituent materials limit the use of solution-processed top electrodes on the HTM/perovskite stacked layer because the device fabrication process requires thermal annealing to evaporate solvents and to fuse metal nanoparticles or nanowires. Therefore, vacuum-evaporated Au and Ag have been commonly employed as top electrodes in perovskite solar cells. In an effort to replace expensive vacuum-deposited top electrodes, several groups have reported fabrication of AgNW-based perovskite solar cells using spray deposition[18–20] and lamination.[21,22] For low-cost perovskite solar cells, the cost-effective, highly conductive copper electrode has recently emerged as a prospective alternative to the silver electrode. Kaltenbrunner et al.[23] demonstrated that a cell with a thermally evaporated Cu contact as an opaque top electrode had an average PCE of 12.5%, which is comparable to that of a cell with an evaporated Au electrode. Shao et al.[24] tried to apply a laminated opaque copper conductive tape to a cell and obtained an average PCE of 11.4% (compared to 14.5% for a cell with a thermally evaporated Al electrode). However, there has been no report on the use of a CuNW top electrode in perovskite solar cells. In this regard, for the first time, we fabricated organometallic halide perovskite solar cells based on CuNW TCEs using Cu–Cu-lactate core–shell nanowires, proving that the feasibility of our reducible fugitive shell derived CuNW TCE as a cost-effective electrode for various optoelectronic applications.

2. Results and Discussion

The CuNWs, measuring 45 ± 5.7 nm in diameter and a few hundred micrometers in length, were synthesized hydrothermally in 1 L batches (≈0.5 g of CuNWs), as shown in **Figure 1**a. The detailed procedures are described in the Experimental Section. The as-prepared CuNWs, synthesized in an aqueous medium under an ambient atmosphere, consisted of a thin native oxide layer on the surface. The intrinsic surface oxide layer was thin enough that it was not detectable by X-ray diffraction (XRD), and the presence of such a small amount of oxide did not have critical influence on the electrical conductivities of CuNW-based TCEs. However, further time-dependent oxidation for a prolonged period would allow the CuNWs to form a thicker oxide layer, leading to increased contact resistance between neighboring nanowires. The surface hydroxide, derived from water molecules, and the chemisorbed residual organics also likely hindered the formation of full contact between the nanowires, deteriorating the electrical transport inside the random networks of nanowire assemblies.

In order to incorporate the surface passivation layer for protection against oxidative reactions as well as to eliminate the surface oxide, surface hydroxide, and organic moieties, the as-synthesized CuNWs were treated with carboxyl acid to create a surface copper carboxylate shell for encapsulating each nanowire. The carboxylic acid reacted with the CuO, Cu_2O, $Cu(OH)_2$, and Cu phases, generating copper carboxylate as a product.[10,25] In general, when sufficient thermal energy is provided, the copper carboxylate is thermally decomposed, with the evaporation of volatile organic phases, and it is reduced to a pure metallic copper phase under an inert atmosphere.[25] The chemical properties of the resulting copper carboxylates are determined predominantly by the kind of carboxylic acid used. When selecting the carboxylic acid, the following factors should be taken into consideration: (i) the carboxylic acid should have moderate acidity in order to form the uniformly conformal copper carboxylate shell layer along the surface of individual nanowires without altering the characteristic 1D morphology; (ii) the copper carboxylate should be insoluble in a certain solvent for stabilizing the resulting carboxylate shell layer as well as preventing the unreacted acid from penetrating the shell layer and reacting with the inner Cu phase; (iii) its decomposition should occur around temperatures at which the junctions between neighboring nanowires are generated; (iv) the decomposition reaction does not involve significant residues and the by-products do not impair the conductivity of networked films.

Based on these considerations, we selected a lactic acid that can produce a copper lactate ($Cu[CH_3CH(OH)COO]_2$) shell layer. The lactic acid was added to the CuNWs dispersed in diethyl ether. The lactic acid could react with copper oxides, a copper hydroxide, or pure copper according to following reactions[10,26]

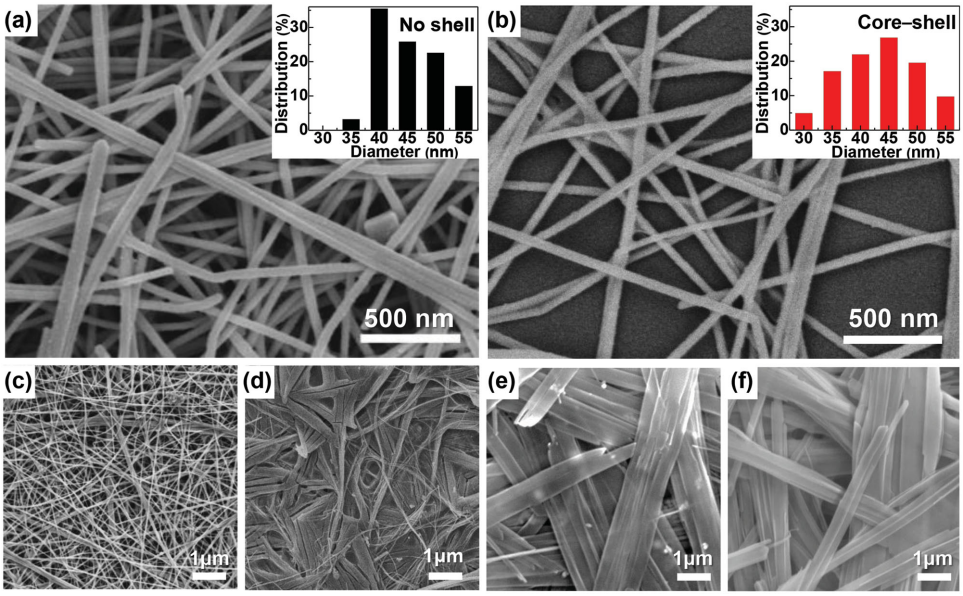

Figure 1. Synthesis of high-quality CuNWs and Cu–Cu-lactate core–shell NWs. a) SEM image of synthesized Cu nanowires. b) SEM image of Cu–Cu-lactate core–shell nanowires. The insets in (a) and (b) show the size distributions of the nanowires. c–f) SEM images of core–shell nanowires prepared by adding different amounts of lactic acid to the suspension containing 0.2 g of CuNWs dispersed in 200 mL of diethyl ether: c) 6.7 mmol; d) 67 mmol; e) 670 mmol; f) 2010 mmol.

$$CuO + 2[CH_3CH(OH)COOH] \rightarrow Cu[CH_3CH(OH)COO]_2 + H_2O \quad (1)$$

$$Cu_2O + 4[CH_3CH(OH)COOH] \rightarrow 2Cu[CH_3CH(OH)COO]_2 + H_2O + H_2 \quad (2)$$

$$Cu(OH)_2 + 2[CH_3CH(OH)COOH] \rightarrow Cu[CH_3CH(OH)COO]_2 + 2H_2O \quad (3)$$

$$Cu + 2[CH_3CH(OH)COOH] \rightarrow Cu[CH_3CH(OH)COO]_2 + H_2 \quad (4)$$

The amount of incorporated lactic acid was controlled to obtain the uniformly conformal and sufficiently thick shell layer. The Scanning electron microscopy image (SEM) images of Cu–Cu-lactate core–shell nanowires are shown in Figure 1b,c; they were formed after 6.7 mmol of lactic acid was added to a 0.016 M CuNW suspension (containing 0.2 g of CuNWs). The 1D morphological structure was well maintained, with a diameter of 43.2 ± 6.9 nm, which indicates that the inner Cu phase was hardly etched. When excessive lactic acid was injected, however, the nanowire morphology gradually collapsed, as shown in Figure 1d–f. The excess acid led to a gradual transformation of the Cu nanowire into a flattened micrometer-sized belt-like Cu lactate, reducing the aspect ratio. The color of the suspension changed from red to pale blue as the concentration of lactic acid was increased (Figure S1, Supporting Information).

The formation of nanowires with a core–shell morphology was confirmed by transmission electron microscope (TEM) images, as shown in **Figure 2**. In the TEM analysis, the nanowires suspended by holey carbon grids were selectively examined to exclude dubious contributions from the TEM grids. The magnified TEM image in Figure 2b clearly reveals that the conformal shell layer uniformly surrounded the CuNW core, demonstrating that each copper nanowire was completely coated by copper lactate with a thickness of ≈3–5 nm. A thicker shell of 8–10 nm was occasionally observed, as shown in Figure S2 (Supporting Information). The edge of the core–shell nanowire was further examined by high-resolution TEM (HR-TEM) analysis to evaluate its crystal structure (Figure 2c). The lattice spacing of 2.08 Å corresponds to the theoretical value for the Cu(111) plane. The lattice distance of 3.2 Å is assigned to copper lactate, which agrees with the value obtained from the XRD spectrum for pure copper lactate (**Figure 3**c). The inverse fast-Fourier-transform (IFFT) pattern (inset of Figure 2c) suggests that the core–shell nanowire consisted of a copper core and a copper lactate shell. In order to clarify the origin of the IFFT ring pattern, we analyzed the XRD patterns of core–shell CuNW films prepared on glass substrates, after they were annealed at 600 °C (high enough to crystallize the amorphous oxide and hydroxide phases) under an inert atmosphere. Only the highly crystallized pure copper phase can be seen in the XRD spectrum, and there are no peaks associated with copper oxides (Figure S3, Supporting Information). In addition, the TEM measurements provide more convincing evidence of the ring pattern. Figure S4 (Supporting Information) shows the selected area electron diffraction (SAED) patterns of the individual bare CuNWs and core–shell CuNWs after annealing at 200 °C under nitrogen atmosphere. As shown in Figure S4a (Supporting Information), the spots in SAED pattern for the bare CuNWs are matched well to the lattice spacing of CuO(111), Cu(111), and Cu(200) (2.4, 2.07, and 1.85 Å, respectively). It is clearly shown that the ring pattern does not

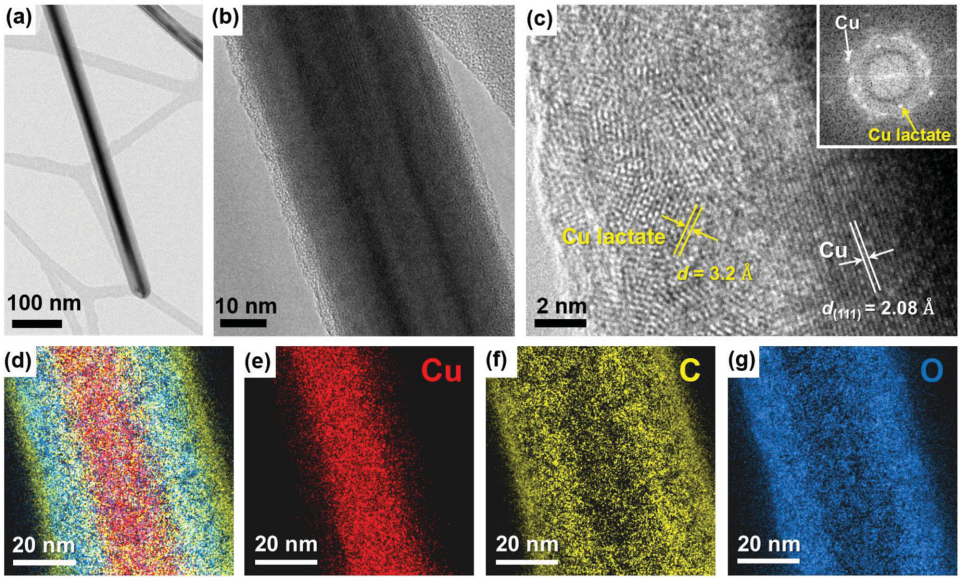

Figure 2. Microstructure of a Cu–Cu-lactate core–shell nanowire. a) TEM image and b) magnified TEM image of a Cu–Cu-lactate core–shell nanowire. c) Corresponding HR-TEM image with an IFFT pattern of the edge of the core–shell nanowire. EF-TEM mapping images with d) all elements, e) elemental copper, f) elemental carbon, and g) elemental oxygen.

exist in bare CuNWs even with the presence of surface oxide layer. For the core–shell CuNWs annealed at 200 °C, the ring pattern disappears and the SAED pattern reveals the presence of presence of Cu(111) and Cu(200) planes of Cu (Figure S4b, Supporting Information). In these regards, it is presumed that the amorphous-like ring pattern is originated not from an amorphous oxide, but from the interfacial region between the inner Cu and outer Cu lactate layers. The lattice arrangement would form a poor heterogeneous interface, and its contribution to the IFFT patterns can be evident in this nanoscale structured material. Elemental distribution analysis was performed on the core–shell nanowire with a 10 nm thick shell layer, in order to observe clearly distinguishable core–shell nanomorphology. Strong intensity of Cu was observed in the core, whereas high intensities of C and O, as well as weak intensity of Cu were observed in the encapsulating shell, as shown in Figure 2d–g. This elemental analysis confirms the formation of uniformly and conformally encapsulated core–shell nanowires.

The thermal behavior of the core–shell nanowires was analyzed by examining the thermogravimetry–differential scanning calorimetry (TG–DSC) measurements, as displayed in Figure 3a. Significant weight loss accompanying an

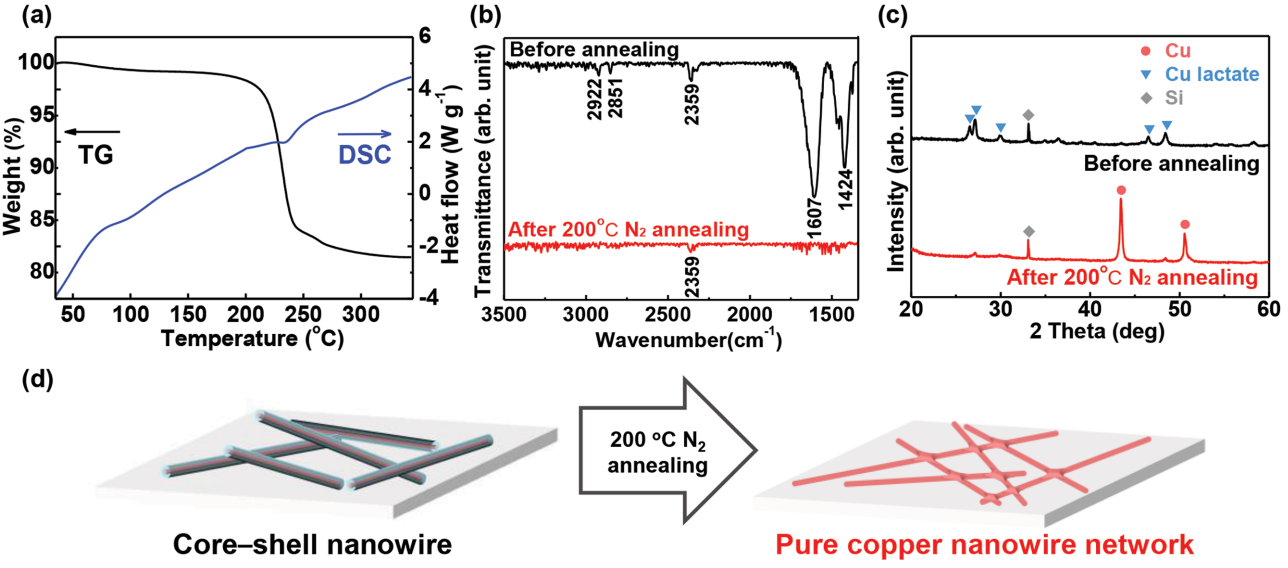

Figure 3. Thermal behavior of Cu–Cu-lactate core–shell nanowires. a) TG–DSC data for core–shell nanowires. b) FT-IR spectroscopy analysis of core–shell nanowires before and after annealing at 200 °C under a nitrogen atmosphere. c) XRD patterns of pure copper lactate before and after annealing at 200 °C under a nitrogen atmosphere. d) Schematic illustration showing the microstructural evolution of core–shell nanowire networks during annealing. The copper lactate shell was reduced to pure Cu, with the formation of well-fused internanowire junctions in the absence of a reductive atmosphere.

endothermal peak occurred at around 200 °C, possibly implying the decomposition of the Cu lactate. Fourier-transform infrared (FT-IR) spectroscopy also allowed us to understand the surface chemical properties of the nanowires (Figure 3b). For the as-synthesized core–shell copper nanowires, the absorption peaks at 1424 and 1607 cm^{-1} correspond to the COO^- symmetric and asymmetric stretching modes, respectively, whereas the peaks at 2851 and 2922 cm^{-1} are attributed to the C—H stretching mode. All these peaks imply the presence of a copper lactate shell. These peaks disappeared from the FT-IR spectrum after the core–shell nanowires were annealed at 200 °C under a nitrogen atmosphere, proving the complete decomposition of the lactate shell layer without leaving any organic residue. The subtle peak at 2359 cm^{-1} observed in the spectra of both samples before and after annealing can be ascribed to the C=O stretching mode of atmospheric CO_2,[27] which is confirmed by the FT-IR spectrum of a clean bare silicon wafer (Figure S5, Supporting Information). We also performed XRD analysis of the pure copper lactate phase, which was synthesized by adding 2010 mmol of lactic acid to the CuNW dispersion (Figure 1f). Before annealing, only the peaks corresponding to copper lactate were observed (the main peak appears at $2\theta = 27.08°$), without the peaks corresponding to the copper phase (Figure 3c). After annealing, only the peaks for the copper phase with a face-centered-cubic structure (Joint Committee on Powder Diffraction Standards (JCPDS) Card No. 04-0836) were observed, suggesting that copper lactate completely decomposed into pure copper. All these findings indicate that the copper lactate shell thermally decomposed and was reduced to pure copper, with volatile gaseous products of carbon dioxide and hydrogen, as well as volatile acetaldehyde (boiling point: 20.2 °C), leaving behind only pure copper[25,26]

$$\mathrm{Cu}\left[\mathrm{CH_3CH(OH)COO}\right]_2 \rightarrow \mathrm{Cu} + 2\mathrm{CO_2}\uparrow + \mathrm{H_2}\uparrow + 2\mathrm{CH_3CHO}\uparrow \quad (5)$$

This endothermal reaction required heat energy to overcome the activation barrier, and the provision of thermal energy at around 200 °C allowed the reaction to take place. This means that annealing the Cu–Cu-lactate core–shell nanowires at 200 °C without a reductive atmosphere enabled us to obtain pure copper nanowires. At the same time, the annealing at 200 °C led to the formation of well-fused junctions, allowing for the formation of TCE films based on highly conductive, pure CuNW networks, as schematically depicted in Figure 3d. A fused internanowire junction between pure CuNWs is shown in Figure S6 (Supporting Information).

The copper lactate shell layer also plays a crucial role in preventing the CuNWs from oxidation during storage. The oxidation stability of the Cu–Cu-lactate core–shell nanowires was investigated by exposing them to different oxidative atmospheres at varying temperatures and levels of relative humidity (RH). The films consisting of metal-nanowire networks were prepared by transferring the vacuum filtrates of either bare Cu or core–shell nanowire dispersions to a glass substrate. After the exposure to each oxidative condition, the films were annealed at 200 °C under a nitrogen atmosphere and the film resistances were measured. **Figure 4**a shows the resistance (R) normalized with respect to the initial value (R_0), as a function of the exposure duration at 25 °C and 30%–45% RH. The sheet resistances of the bare copper-nanowire films soared by a factor of 2.4×10^4 within 72 d, while the core–shell-nanowire films showed little change in sheet resistance. Even under severe oxidative conditions at 70 °C and 70%–75% RH, R/R_0 of the core–shell-nanowire films was only about 1.77, whereas the bare-CuNW films degraded more abruptly, as indicated by the resistance that was 6.8×10^5 times higher after 72 h (Figure 4b). XRD analysis also confirmed the antioxidation stability of the core–shell nanowires; the copper oxide peak was observed in the pattern of the bare-CuNW film after 72 h exposure at 70 °C and 70%–75% RH, whereas the core–shell-nanowire film lacked the oxide phase (Figure 4c). TG–DSC analysis carried out in air clearly revealed that the bare CuNWs gradually gained weight with increasing temperature through a thermally activated oxidation reaction, while the core–shell CuNWs showed almost no weight gain prior to the shell decomposition at 200 °C (Figure 4d).

Various deposition methods have been employed to fabricate nanowire-based transparent conductors, including vacuum filtration,[10,28–30] spin coating,[31] spray coating,[32–34] Meyer rod coating,[35–37] and doctor blading.[38,39] Among them, spray deposition has been recognized as a simple, scalable method that is well suited even to curved, irregularly shaped surfaces as well as large-area planar surfaces. To realize reproducible high-quality CuNW-based TCEs by spray deposition, the CuNWs should be well dispersed in a solvent to form a stable and easily sprayable nanowire ink. The dispersion of CuNWs in a solvent might raise the possibility of oxidization akin to that during storage under an ambient atmosphere, so the CuNWs must maintain their antioxidation stability in the dispersion (ink) for practical utilization in various applications. Unlike highly surface-activated bare Cu nanowires, the Cu–Cu-lactate core–shell nanowires can be processed into well dispersed, stable nanowire inks (over 1 month in air) with high antioxidation capability (Figure S7, Supporting Information).

The schematic diagram of the spraying procedure is illustrated in **Figure 5**a. We prepared the easily sprayable core–shell nanowire ink by adding isopropyl alcohol to a diethyl-ether-based CuNW dispersion, with which highly transparent, uniform CuNW-network films were obtained in a large area, as shown in Figure 5b. The transparency of the CuNW films was controlled by adjusting the dispersion concentration and the spraying parameters. The as-prepared core–shell CuNW network had high resistance to some extent, since the copper lactate shell employed for protecting inner conductive copper core is not conductive but rather insulating. After annealing the as-spray-coated films, the lactate shell was reduced to pure Cu, and the pure CuNW films exhibited good optoelectrical properties, with a low sheet resistance of $19.8 \pm 0.9\ \Omega\ sq^{-1}$ and a high optical transmittance of 85.5% at a wavelength of 550 nm, which are comparable to results obtained by hydrogen reductive annealing techniques (Figure 5c).[12,29,30,36] To compare the long-term storage stability, both bare-CuNW and core–shell-CuNW dispersions were stored for a prolonged period under an ambient atmosphere. The optoelectrical properties of films were evaluated after they were annealed at 200 °C. The transparent electrodes prepared from the core–shell-CuNW ink maintained their performance even when 21-d-old ink was used

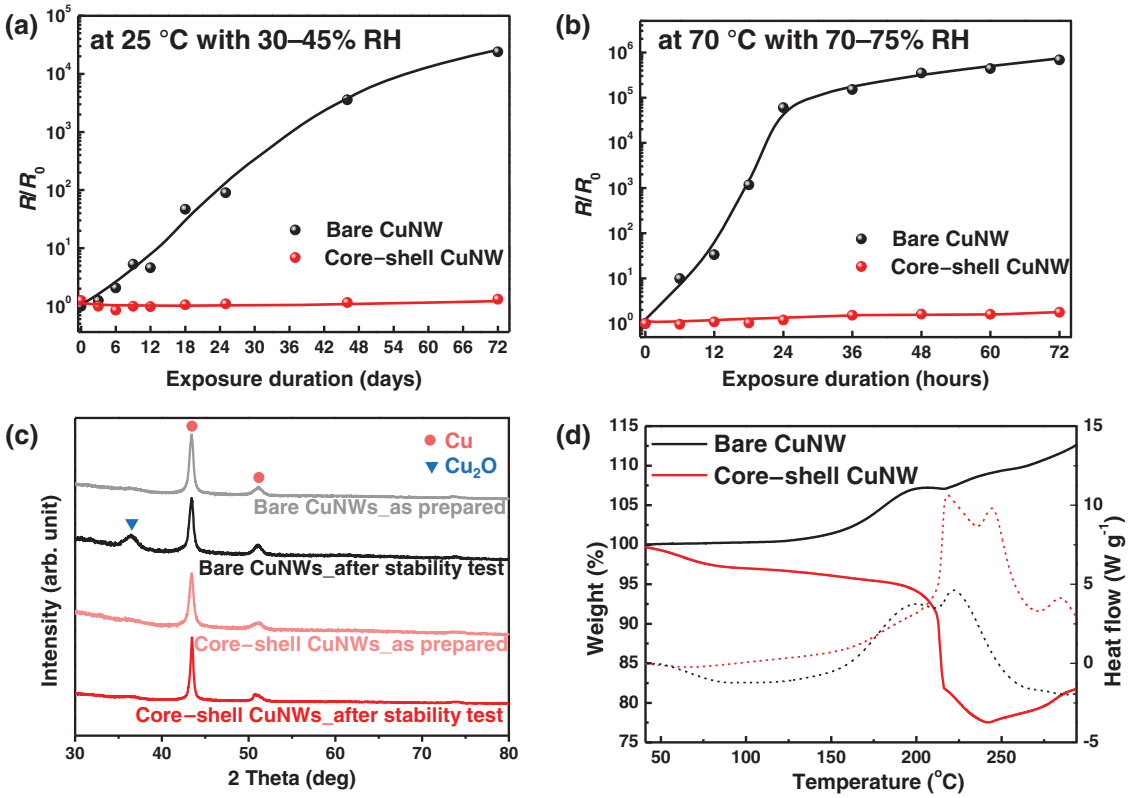

Figure 4. Thermal stability of Cu–Cu-lactate core–shell nanowires. Relative resistance (R/R_0) as a function of exposure duration at different temperatures and under different levels of humidity in air: a) 25 °C, 30%–45% RH; b) 70 °C, 70%–75% RH. For all samples, the sheet resistances were measured after annealing at 200 °C under a N_2 atmosphere. c) XRD patterns of as-synthesized bare CuNWs and core–shell nanowires before and after 72 h exposure at 70 °C and 70%–75% RH. d) TG–DSC results in air for as-synthesized bare CuNWs and core–shell nanowires.

(Figure 5d). In contrast, the basic performance of the TCEs prepared from the bare-CuNW ink was significantly degraded owing to gradual oxidation, as the ink was stored for an extensive period (Figure 5e). As confirmed by the XRD results, the films prepared from the 21-d-old bare-CuNW ink showed a Cu oxide peak, while the film obtained from the 21-d-old core–shell-CuNW ink did not show any oxide peaks (Figure S8, Supporting Information). These results clearly prove that the copper lactate shell would be a viable protective layer against oxidation in solvents, ensuring sufficient shelf life.

Using Cu–Cu-lactate core–shell nanowires, we demonstrate here, for the first time, the feasibility of CuNW TCEs for application in organometallic halide perovskite solar cells. A transparent top electrode is a requisite constituent of semitransparent perovskite solar cells, and it is also applicable to tandem cells, windows, or rooftops. Both the anode and cathode should be transparent in a semitransparent device. To date, the most commonly used transparent top electrodes are vacuum-sputtered ITOs and silver nanowires; but, both indium and silver are expensive metals. Since the organometallic halide perovskite and spiro-OMeTAD layers are degraded at the Cu-lactate decomposition temperature (200 °C), and a spraying solvent can dissolve both the perovskite and spiro-OMeTAD layers, we selected the annealing-free and solvent-free lamination method rather than direct spraying to deposit CuNWs as a top contact on perovskite devices.[21,22] The core–shell-CuNW TCEs (sheet resistance of 17–24 Ω sq^{-1} and optical transmittance of 82.8% at a wavelength of 550 nm) were transferred onto the spiro-OMeTAD/$CH_3NH_3PbI_3$/TiO_2/FTO (fluorine-doped tin oxide) device stacks through a ball bearing technique. Although the resistance of CuNW TCEs was increased slightly by a factor of 3–5 after lamination as a result of the manual-process-driven nonuniform pressure distribution in the overall area, the average resistance was still acceptable as a top electrode. The schematic structure of a CuNW-based perovskite solar cell is illustrated in **Figure 6**a. Figure 6b shows the uniformly deposited CuNW networks on top of the p–n junction. For comparison, a perovskite solar cell with a sputtered ITO electrode (sheet resistance of 20.1 Ω sq^{-1} and optical transmittance of 87.2% at a wavelength of 550 nm) was fabricated with a MoO_x layer to suppress the damage to spiro-OMeTAD/$CH_3NH_3PbI_3$ during sputtering. The combined ITO/MoO_x layer showed a sheet resistance of 20.8 Ω sq^{-1} and optical transmittance of 82.3% at 550 nm. The photovoltaic performance of perovskite solar cells with either a CuNW or ITO top electrode, which were fabricated under identical processes except for the transparent electrode, are shown in Figure 6c,d; the performance parameters are summarized in **Table 1**. The best reference ITO cell showed a PCE of 13.39%, open-circuit voltage (V_{OC}) of 1.03 V, short-circuit current (J_{SC}) of 19.49 A cm^{-2}, and fill factor (FF) of 66.69%. The CuNW-based champion perovskite solar cell exhibited a PCE of 9.88%, V_{OC} of 0.95 V, J_{SC} of 19.10 A cm^{-2}, and FF of 54.57%. Both solar cells exhibited hysteresis during positive scanning ($J_{SC} \rightarrow V_{OC}$) or negative

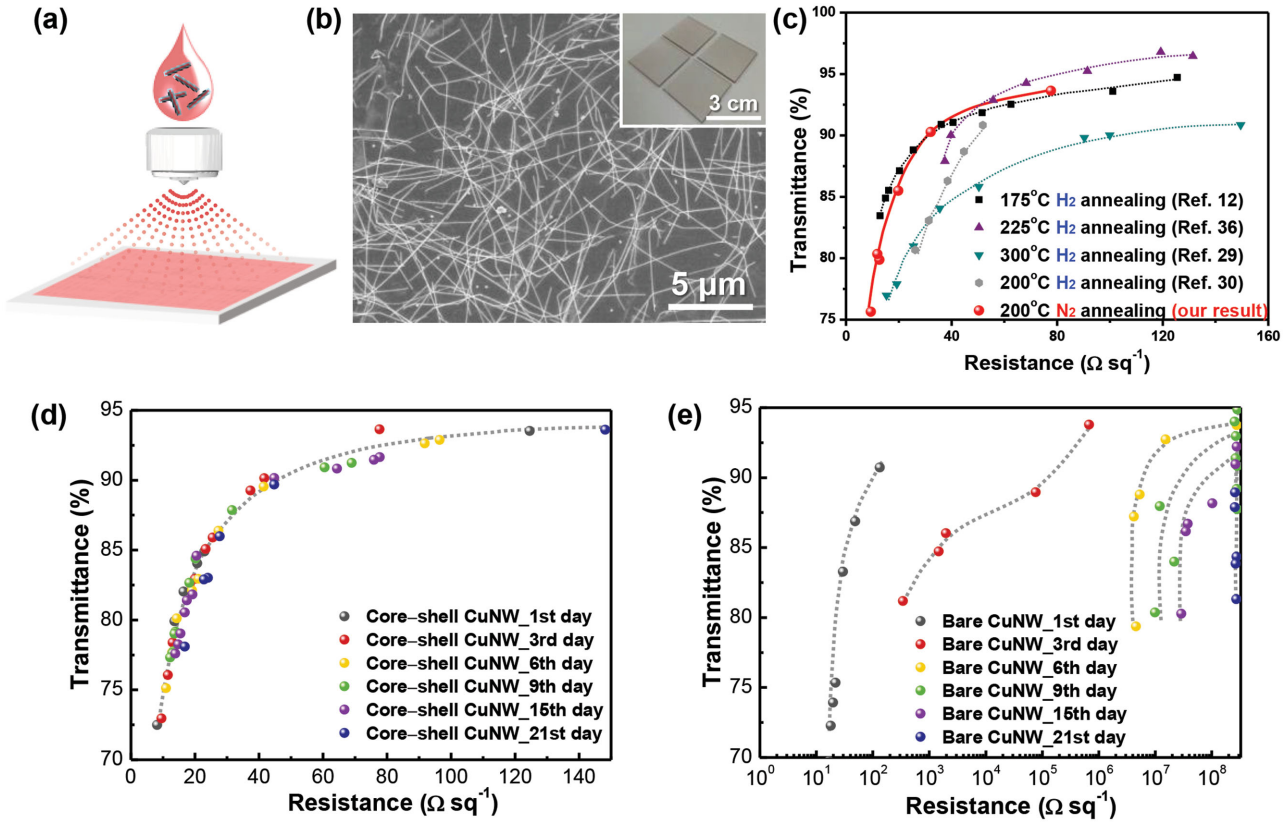

Figure 5. TCE prepared from core–shell-CuNW ink and its long-term storage stability. a) Schematic illustration of spraying process to produce nanowire-network films. b) SEM image of a sprayed, core–shell CuNW-based TCE; the inset is a photograph of fabricated CuNW TCEs. c) Sheet resistance versus optical transmission (at 550 nm) of sprayed, reducible shell-derived TCEs, compared with values reported for TCEs prepared with hydrogen heat-treatment. The optical (at 550 nm) and electrical properties of TCEs derived from d) core–shell-CuNW ink and e) bare-CuNW ink as functions of storage time. Each film was sprayed from 1-, 3-, 6-, 9-, 15-, or 21-d-old ink.

scanning ($V_{OC} \rightarrow J_{SC}$) with a delay time of 50 ms and scan speed of 520 mV s^{-1} (Figure S9, Supporting Information). The reduction in efficiency of the CuNW-TCE-based perovskite cells is attributable to an increase in series resistance and a decrease of shunt resistance, as expressed by significant FF drop; since the lamination procedure was manually performed, it was possible that there was an incomplete transfer or a disconnection of the nanowire networks, resulting in the increase of series resistance with a drop in J_{SC}. In addition, the local uneven perpendicular force would have resulted in the formation of a partial shunting path by causing the 1D nanowires to penetrate the underlying HTM and perovskite layers, which likely caused a drop in shunt resistance and a decrease in V_{OC}. Despite the slightly lower PCE, the beauty of our study is to demonstrate the potential suitability of CuNWs as a vacuum-free and noble-metal-free electrode for ultralow-cost perovskite solar cells. It is highly believed that the device performance parameters could be further improved with a sophisticatedly controlled lamination process.

3. Conclusions

We fabricated highly conductive, transparent CuNW network films using a (reducible and oxidant-resistant fugitive) Cu-lactate-based core–shell-CuNW ink. The uniformly conformal Cu carboxylate shell layer encapsulating individual CuNWs was obtained via simple one-pot synthesis by adding lactic acid to the as-prepared CuNW suspension. The copper lactate was reduced to a pure metallic copper phase and well-fused junctions were formed upon annealing at 200 °C without the provision of a reductive atmosphere. It was revealed that the CuNW TCE films were highly transparent (optical transmittance of 85.5% at a wavelength of 550 nm) and conductive (sheet resistance of 19.8 ± 0.9 Ω sq^{-1}), and their optoelectrical properties were comparable to those of transparent conductive films obtained to date by hydrogen reductive annealing techniques. Most importantly, it was clearly demonstrated that the core–shell CuNWs had long-term storage stability as the copper lactate shell readily protected the pure Cu core from oxidation in air or in a solvent. Furthermore, we demonstrated, for the first time, successful fabrication of vacuum-free and noble-metal-free CuNW electrodes for ultralow-cost perovskite solar cells. The highly conductive CuNW networks were successfully transferred onto the top of perovskite devices, and the resulting PCE of 9.88% is comparable to the PCE (13.39%) of conventional sputtered-ITO-based perovskite solar cells. These results clearly show the potential of our reducible fugitive shell-based CuNWs for application as an inexpensive electrode in various optoelectronic devices.

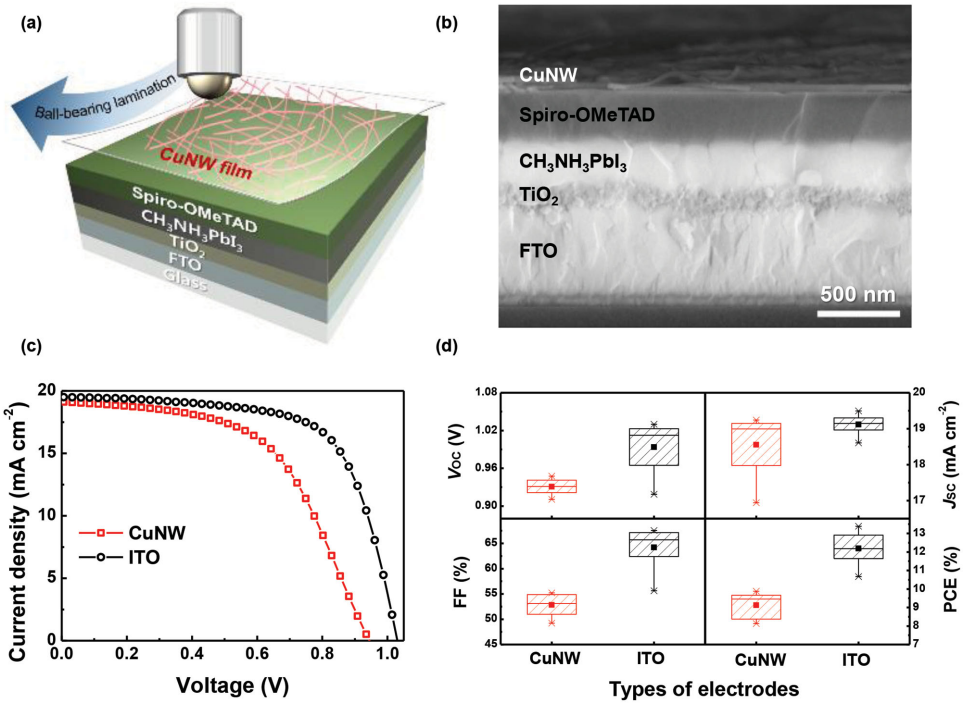

Figure 6. Perovskite solar cells with CuNW TCEs. a) Schematic structure and b) SEM cross-sectional image of a perovskite solar cell employing copper-nanowire networks as a top electrode. c) Current density–voltage (*J*–*V*) curves of devices with electrodes based on transferred CuNWs and sputtered ITO. d) Statistics of the device parameters, V_{OC}, J_{SC}, FF, and PCE, gathered from eight cells of CuNW- and ITO-based devices. The 25th, 50th, and 75th percentiles of the device parameters are presented with the three horizontal lines in the box. The average and maximum/minimum values are denoted by ■ and ×, respectively.

4. Experimental Section

Synthesis of Copper-Nanowire Solution: In order to prepare the precursor solution for the chemical reaction to form the copper nanowires, 0.013 M of anhydrous copper chloride ($CuCl_2$; 97%, Sigma-Aldrich, St Louis, MO, USA), 0.011 M of anhydrous dextrose ($C_6H_{12}O_6$; Sigma-Aldrich), and 0.056 M of 1-hexadecylamine ($C_{16}H_{35}N$; 98%, Sigma-Aldrich) were dissolved in 600 mL of deionized water. The solution was stirred at 600 rpm for 12 h to obtain a well-dispersed Cu(II)–alkyl amine complex.[40] The sky-blue-colored emulsion was then heated in a hydrothermal reactor at 120 °C for 15 h. When the reaction was completed, a reddish-brown aqueous CuNW suspension was obtained. The solution was centrifuged for 4 min at 12 000 rpm and then washed several times with deionized water and a 1:2 (vol) mixture of isopropyl alcohol (IPA; Duksan Pure Chemicals, Ansan-si, Gyeonggi-do, Korea) and hexane (Duksan Pure Chemicals) to remove unreacted residues.

Synthesis of Core–Shell-Copper-Nanowire Ink: The washed CuNW was dispersed in diethyl ether. The suspension was briefly ultrasonicated for 6 min and 0.3 wt% of dispersing agent (BYK 2163; BYK-Chemie GmbH, Wesel, Germany) was added to improve the dispersity. Then 0.2 g of the CuNW were dispersed in 200 mL of diethyl ether, and 6.7 mmol of lactic acid was injected, followed by stirring at 600 rpm for 4 h. After completion of the reaction, the core–shell CuNWs were washed several times with diethyl ether to remove any remaining acid and organic residues. Finally, the resulting products were redispersed in diethyl ether to form a suspension with core–shell CuNW concentration of 0.063 M.

Thermal Stability Test: Both bare-CuNW and core–shell-CuNW suspensions were vacuum-filtered through membranes (mixed cellulose ester membrane filter with a diameter of 25 mm and a pore diameter of 1.0 μm, Advantec, Bunkyo-ku, Tokyo, Otowa, Japan). The filtered solids were then transferred onto glass substrates, followed by rinsing with acetone to remove residual components of the membrane. The prepared films were exposed to two different sets of atmospheric conditions—30%–45% RH at 25 °C and 70%–75% RH at 70 °C—for different durations. After atmospheric exposure under each oxidative condition, the films were annealed at 200 °C for 30 min under a nitrogen atmosphere prior to the sheet-resistance measurements.

Fabrication of CuNW TCEs: CuNW-based TCE films were prepared by spraying the copper-nanowire ink onto the substrates of interest. Prior to spraying, the core–shell CuNWs in the diethyl-ether-based dispersion were diluted with IPA to improve the dispersion stability and to adjust the nanowire concentration so that the suspension would be suitable for spraying. The CuNWs were deposited on 3 × 3 cm^2 glass substrates via spray coating. The spray pressure was 0.2 MPa and the substrate was heated at 45 °C during the spray-deposition process. After film fabrication, the films were annealed at 200 °C for 30 min on a hot plate under a nitrogen atmosphere prior to film evaluation.

Characterizations: The surface and cross-sectional images of the CuNW network and perovskite solar cell were obtained by a

Table 1. Performance metrics of champion and average values for perovskite cells with either CuNW or ITO top electrode.

Electrode type		V_{OC} [V]	J_{SC} [mA cm^{-2}]	FF [%]	PCE [%]
CuNW	Champion	0.95	19.10	54.57	9.88
	Average	0.93 ± 0.01	18.55 ± 0.84	52.81 ± 2.23	9.13 ± 0.71
ITO	Champion	1.03	19.49	66.69	13.39
	Average	0.99 ± 0.05	19.12 ± 0.28	64.21 ± 4.17	12.19 ± 0.92

field-emission scanning electron microscope (JEOL-6701F, JEOL Inc.,Tokyo, Japan). HR-TEM (JEM-ARM200F, JEOL Inc.), together with elemental mapping via energy-filtered transmission electron microscopy (EF-TEM), was used to analyze the core–shell microstructure. The crystal structure of the core–shell nanowires was determined by an X-ray diffractometer (D/MAX-2500, Rigaku, Tokyo, Japan). FT-IR spectroscopy (Vertex70, Bruker Optics Inc., Billerica, MA, USA) was used to investigate the absorbed chemical species of both core–shell and bare CuNWs. The thermal behavior of the core–shell and bare CuNWs were measured via thermogravimetry coupled with differential scanning calorimetry (SDT Q600, TA Instruments, New Castle, DE, USA) under an inert or ambient gas flow (100 cm^3 min^{-1}) at a heating rate of 5 °C min^{-1}. The sheet resistances were determined via a four-point probe system (RS8, BEGA Technologies, Seoul, Korea), and the optical transmittances (T) of the CuNW films were measured by an ultraviolet–visible (UV–vis) spectrophotometer (V-530, JASCO, Tokyo, Japan), using a baseline obtained with clean soda-lime glass.

Fabrication of Organometallic Halide Perovskite Solar Cell: We applied the CuNW-based TCEs to organometallic halide perovskite solar cells. For comparison, a perovskite cell with an ITO electrode was also fabricated as a control sample, while all the underlying layers were identical. To fabricate the perovskite solar cells, we followed Lewis base adduct method proposed by Ahn et al.[41] A compact mesoporous hole-blocking TiO_2 layer was spin coated on FTO glass: a 0.15 M TiO_2 nanoparticle solution was first formed by diluting titanium diisopropoxide bis(acetylacetonate) (75 wt% in isopropanol, Sigma-Aldrich) with 1-butanol, this solution was then spin coated at 2000 rpm for 20 s, followed by drying at 125 °C for 5 min and then annealing at 550 °C for 1 h. An aqueous 20×10^{-3} M $TiCl_4$ (Sigma-Aldrich, >98%) solution was used to treat the TiO_2-coated substrate at 90 °C for 10 min, which was then annealed at 500 °C for 30 min. Next, the perovskite absorber layer was fabricated with a 53 wt% mixture of PbI_2, CH_3NH_3I, and dimethyl sulfoxide (Sigma-Aldrich) (1:1:1 molar ratio) in dimethylformamide (Sigma-Aldrich): the precursor solution was spin coated at 4000 rpm for 25 s, followed by drying at 65 °C for 3 min and annealing at 105 °C for 10 min. The hole-transporting layer was prepared as follows: the precursor solution for the HTM was prepared by using 54×10^{-3} M of 2,2′,7,7′-tetrakis(*N*,*N*-di-*p*-methoxyphenylamine)-9,9-spirobifluorene (spiro-OMeTAD, Boron Molecular, Raleigh, NC, USA) in chlorobenzene, with 177.7×10^{-3} M of 4-tert-butylpyridine and 28.5×10^{-3} M of lithium bis-(trifluoromethylsulfonyl)imide in acetonitrile as additives; the solution was spin coated at 1150 rpm for 30 s. We used CuNW films with 82.8% transmittance at 550 nm to fabricate the top electrode by transferring the lamination onto the HTM. For better lamination, a hydrophobic self-assembled monolayer was coated for chemical modification of the polyimide (PI) substrate donor. The PI films were functionalized with 1*H*,1*H*,2*H*,2*H*-perfluorodecyltriethoxysilane (FDTS, 97%, Alfa Aesar, Ward Hill, MA, USA) by immersing them in a 10×10^{-3} M FDTS–*n*-hexane solution, and after 24 h, the films were rinsed several times with hexane and ethanol. The CuNWs were deposited by spraying the CuNW suspension, following the same procedure used for CuNW-TCE fabrication. The CuNW-coated PI film was placed on the HTM, and the CuNW network was transfer laminated by applying gentle pressing with ball bearings to complete the cell fabrication. For comparison, an evaporated MoO_x (5 nm)/sputtered ITO (329 nm) electrode was deposited on top of the HTM layer.

Device Characterization: The performances of perovskite solar cells based on both CuNW and ITO transparent electrodes were evaluated by analyzing their current density–voltage (J–V) characteristics with a solar simulator (Sol3A Class AAA, Oriel Instruments, Stratford, CT, USA) and a Keithley 2400 source measurement unit (Keithley Instruments Inc., Cleveland, OH, USA) under air mass (AM) 1.5 and 1 sun (100 mW cm^{-2}) conditions; the intensity was calibrated with a standard Si reference cell certified by Newport Corporation (Irvine, CA, USA). The perovskite solar cells were illuminated through a 0.06 cm^2 of mask aperture. The scan rate was 0.52 V s^{-1}, from –0.1 to 1.2 V, with a dwell time of 50 ms for each point.

Supporting Information

Supporting Information is available from the Wiley Online Library or from the author.

Acknowledgements

This work was supported by a National Research Foundation of Korea (NRF) grant funded by the Korea government (Grant No. 2012R1A3A2026417).

Received: April 26, 2016
Revised: June 29, 2016
Published online: August 16, 2016

[1] W.-K. Kim, S. Lee, D. H. Lee, I. H. Park, J. S. Bae, T. W. Lee, J.-Y. Kim, J. H. Park, Y. C. Cho, C. R. Cho, S.-Y. Jeong, *Sci. Rep.* **2015**, *5*, 10715.
[2] F. Cui, Y. Yu, L. Dou, J. Sun, Q. Yang, C. Schildknecht, K. Schierle-Arndt, P. Yang, *Nano Lett.* **2015**, *15*, 7610.
[3] A. R. Rathmell, B. J. Wiley, *Adv. Mater.* **2011**, *23*, 4798.
[4] S. Li, Y. Chen, L. Huang, D. Pan, *Inorg. Chem.* **2014**, *53*, 4440.
[5] J. Chen, J. Chen, Y. Li, W. Zhou, X. Feng, Q. Huang, J.-G. Zheng, R. Liu, Y. Ma, W. Huang, *Nanoscale* **2015**, *7*, 16874.
[6] R. Lin, S. Zhang, Z. Du, H. Fang, Y. Ren, X. Wu, *RSC Adv.* **2015**, *5*, 87090.
[7] D. Han, X. Li, X. Zhao, J. Feng, Y. Qian, *J. Nanosci. Nanotechnol.* **2015**, *15*, 7177.
[8] C. Hwang, T.-H. Kim, Y.-G. Cho, J. Kim, H.-K. Song, *Sci. Rep.* **2015**, *5*, 8623.
[9] C. Sachse, N. Weiß, N. Gaponik, L. Müller-Meskamp, A. Eychmüller, K. Leo, *Adv. Energy Mater.* **2014**, *4*, 1300737.
[10] Y. Won, A. Kim, D. Lee, W. Yang, K. Woo, S. Jeong, J. Moon, *NPG Asia Mater.* **2014**, *6*, e105.
[11] Z. Chen, A. R. Rathmell, S. Ye, A. R. Wilson, B. J. Wiley, *Angew. Chem.* **2013**, *125*, 13953.
[12] I. E. Stewart, A. R. Rathmell, L. Yan, S. Ye, P. F. Flowers, W. You, B. J. Wiley, *Nanoscale* **2014**, *6*, 5980.
[13] S. Han, S. Hong, J. Ham, J. Yeo, J. Lee, B. Kang, P. Lee, J. Kwon, S. S. Lee, M.-Y. Yang, S. Ko, *Adv. Mater.* **2014**, *26*, 5808.
[14] S. Han, S. Hong, J. Yeo, D. Kim, B. Kang, M.-Y. Yang, S. Ko, *Adv. Mater.* **2015**, *27*, 6397.
[15] D. Paeng, J.-H. Yoo, J. Yeo, D. Lee, E. Kim, S. Ko, C. P. Grigoropoulos, *Adv. Mater.* **2015**, *27*, 2762.
[16] H. Kang, E. Sowade, R. R. Baumann, *ACS Appl. Mater. Interfaces* **2014**, *6*, 1682.
[17] Best Research-Cell Efficiencies, http://www.nrel.gov/ncpv/images/efficiency_chart.jpg (accessed: 20 April 2016).
[18] F. Guo, H. Azimi, Y. Hou, T. Przybilla, M. Hu, C. Bronnbauer, S. Langner, E. Spiecker, K. Forberich, C. J. Brabec, *Nanoscale* **2015**, *7*, 1642.
[19] M. Lee, Y. Ko, B. K. Min, Y. Jun, *ChemSusChem* **2016**, *9*, 31.
[20] K. Yang, F. Li, J. Zhang, C. P. Veeramalai, T. Guo, *Nanotechnology* **2016**, *27*, 095202.
[21] C. D. Bailie, M. G. Christoforo, J. P. Mailoa, A. R. Bowring, E. L. Unger, W. H. Nguyen, J. Burschka, N. Pellet, J. Z. Lee, M. Grätzel, R. Noufi, T. Buonassisi, A. Salleo, M. D. McGehee, *Energy Environ. Sci.* **2015**, *8*, 956.
[22] J. P. Mailoa, C. D. Bailie, E. C. Johlin, E. T. Hoke, A. J. Akey, W. H. Nguyen, M. D. McGehee, T. Buonassisi, *Appl. Phys. Lett.* **2015**, *106*, 121105.

[23] M. Kaltenbrunner, G. Adam, E. D. Glowacki, M. Drack, R. Schwödiauer, L. Leonat, D. H. Apaydin, H. Groiss, M. C. Scharber, M. S. White, N. S. Sariciftci, S. Bauer, *Nat. Mater.* **2015**, *14*, 1032.
[24] Y. Shao, Q. Wang, Q. Dong, Y. Yuan, J. Huang, *Nano Energy* **2015**, *16*, 47.
[25] I. Kim, Y. Kim, K. Woo, E.-H. Ryu, K.-Y. Yon, G. Cao, J. Moon, *RSC Adv.* **2013**, *3*, 15169.
[26] D. Deng, Y. Cheng, Y. Jin, T. Qi, F. Xiao, *J. Mater. Chem.* **2012**, *22*, 23989.
[27] R. N. Mariammal, N. Rajamanickam, K. Ramachandran, *J. Nano-Electron. Phys.* **2011**, *3*, 92.
[28] L. Shi, R. Wang, H. Zhai, Y. Liu, L. Gao, J. Sun, *Phys. Chem. Chem. Phys.* **2015**, *17*, 4231.
[29] D. Zhang, R. Wang, M. Wen, D. Weng, X. Cui, J. Sun, H. Li, Y. Lu, *J. Am. Chem. Soc.* **2012**, *134*, 14283.
[30] J. Song, J. Li, J. Xu, H. Zeng, *Nano Lett.* **2014**, *14*, 6298.
[31] Y. Ahn, Y. Jeong, D. Lee, Y. Lee, *ACS Nano* **2015**, *9*, 3125.
[32] F. Selzer, N. Weiß, D. Kneppe, L. Bormann, C. Sachse, N. Gaponik, A. Eychmüller, K. Leo, L. Müller-Meskamp, *Nanoscale* **2015**, *7*, 2777.
[33] D. Y. Choi, H. W. Kang, H. J. Sung, S. S. Kim, *Nanoscale* **2013**, *5*, 977.
[34] I. N. Kholmanov, S. H. Domingues, H. Chou, X. Wang, C. Tan, J.-Y. Kim, H. Li, R. Piner, A. J. G. Zarbin, R. S. Ruoff, *ACS Nano* **2013**, *7*, 1811.
[35] Z. Chen, S. Ye, I. E. Stewart, B. J. Wiley, *ACS Nano* **2014**, *8*, 9673.
[36] S. Ye, A. R. Rathmell, I. E. Stewart, Y.-C. Ha, A. R. Wilson, Z. Chen, B. J. Wiley, *Chem. Commun.* **2014**, *50*, 2562.
[37] I. E. Stewart, S. Ye, Z. Chen, P. F. Flowers, B. J. Wiley, *Chem. Mater.* **2015**, *27*, 7788.
[38] F. Guo, P. Kubis, T. Przybilla, E. Spiecker, A. Hollmann, S. Langner, K. Forberich, C. J. Brabec, *Adv. Energy Mater.* **2015**, *5*, 1401779.
[39] F. Guo, P. Kubis, T. Stubhan, N. Li, D. Baran, T. Przybilla, E. Spiecker, K. Forberich, C. J. Brabec, *ACS Appl. Mater. Interfaces* **2014**, *6*, 18251.
[40] D. V. R. Kumar, I. Kim, Z. Zhong, K. Kim, D. Lee, J. Moon, *Phys. Chem. Chem. Phys.* **2014**, *16*, 22107.
[41] N. Ahn, D.-Y. Son, I.-H. Jang, S. M. Kang, M. Choi, N.-G. Park, *J. Am. Chem. Soc.* **2015**, *137*, 8696.